Available online at www.sciencedirect.com
ScienceDirect
Trans. Nonferrous Met. Soc. China 28(2018) 1149−1156
Transactions of Nonferrous Metals Society of China
www.tnmsc.cn

Effect of heat treatment on corrosion properties of CuAlNi shape memory alloy

L. VRSALOVIĆ[1], I. IVANIĆ[2], S. KOŽUH[2], S. GUDIĆ[1], B. KOSEC[3], M. GOJIĆ[2]

1. Department of Electrochemistry and Materials Protection, Faculty of Chemistry and Technology, University of Split, Ruđera Boškovića 35, 21000 Split, Croatia;
2. Faculty of Metallurgy, University of Zagreb, Aleja narodnih heroja 3, 44103 Sisak, Croatia;
3. Faculty of Natural Sciences and Engineering, University of Ljubljana, Aškerčeva cesta 12, 1000 Ljubljana, Slovenia

Received 29 April 2017; accepted 4 August 2017

Abstract: The effect of heat treatment on corrosion properties of CuAlNi shape memory alloy was investigated in 0.9% NaCl solution at pH 7.4 and 37 °C by open circuit potential measurements, polarisation techniques, and electrochemical impedance spectroscopy. Investigations were performed on CuAlNi alloy samples in as-cast state and after heat treatment procedure containing annealing at 850, 885 and 920 °C followed by water quenching. Electrochemical impedance measurement results indicate that heat treatment of CuAlNi alloy leads to the increase in charge transfer resistance and surface layer resistance and the decrease in values of capacitance of the double and surface layers, indicating higher corrosion resistance compared with the as-cast CuAlNi alloy. The increase in polarisation resistance and the decrease in corrosion current density of heat-treated CuAlNi alloy also suggest beneficial influence of heat treatment on corrosion resistance of CuAlNi alloy. Optical microscopy, SEM/EDX and XRD analysis of samples surface after polarisation measurements show the occurrence of pitting corrosion on the electrode surfaces, with the existence of $CuCl_2$, $AlCl_3$ and $Cu_2Cl(OH)_3$ compounds as the surface corrosion products.
Key words: CuAlNi alloy; corrosion; polarisation; electrochemical methods; SEM

1 Introduction

Copper–nickel alloy has great practical application as condenser tubes for ships, heat exchangers of power plant, pipeline networks and other structures engineered for industry and for marine use, due to its good mechanical workability, excellent electrical and thermal conductivity, and good resistance to corrosion [1−3]. Addition of Al to copper−nickel alloy results in higher corrosion resistance of alloy, especially in sulphuric acid, salt solutions, or high temperature environments [4−7]. Besides, CuAlNi alloy presents shape memory effect in alloys with aluminium content close to 14% (mass fraction) [8]. Shape memory alloy (SMA) remembers its original shape returning the pre-deformed shape upon heating above certain temperature. The key characteristic responsible for this behaviour is the occurrence of a martensitic phase transformation which is shear-dominant diffusionless solid state phase transformation from a parent austenitic phase [9,10]. The four characteristic temperatures of this diffusionless phase transformation are A_s, A_f, M_s and M_f. A_s represents the temperature at which austenite begins to form, and A_f is the temperature at which all martensite has transformed to austenite. On the other hand, austenite begins to transform in martensite during cooling (M_s) until only martensite is left (M_f). These temperatures basically define the temperature regime in which SMAs can be employed [11].

Due to their versatile specific properties, shape memory alloys are commonly used in medical and industrial engineering applications. The medical applications include eyeglass frames, surgical stents, orthodontic arch wires, and active catheters. The industrial engineering applications include manufacturing of actuators, sensors and microelectro-mechanical systems (MEMS), functional devices such as fasteners, sealing and coupling, cellular phone antennas, fuel injectors and small helicopter rotors [10,12,13].

Nitinol (NiTi) is the most popular and the most commonly used SMA due to its superior thermo-mechanical and thermoelectrical properties, greater shape memory strain, and better corrosion resistance

Corresponding author: L. VRSALOVIĆ; Tel: +385-21329444; E-mail: ladislav@ktf-split.hr
DOI: 10.1016/S1003-6326(18)64752-1

compared with Cu-based alloys. Nevertheless, NiTi alloys have lower transformation temperatures (from −100 to 100 °C) which decrease strongly with increasing Ni content [14], and also much higher production cost compared with Cu-based alloys [5,9,15,16].

Good electrical and thermal conductivity along with their formability makes Cu-based shape memory alloys an attractive alternative to NiTi alloys [17]. CuAlNi alloys have some considerable advantages over Ni−Ti such as less difficult melting, casting, and composition control, higher elastic modulus, better work/cost ratio, better machinability and transformation temperature in a range from −200 and 200 °C depending on Al and Ni content [16,18,19]. HUSAIN and CLAPP [8] found that CuAlNi alloy in the polycrystalline state is brittle and therefore cannot be easily worked due to the high degree of order and high elastic anisotropy of the parent β-phase. This anisotropy is more pronounced in coarse-grained Cu-based shape memory alloys, which are generally produced under relatively low cooling rates [13,17,20]. The grain size of Cu−Al−Ni alloys produced by the conventional casting methods can be large as several millimeters [21]. Therefore, the brittleness is a severe problem in the cast Cu−Al−Ni alloys due to the large grain size coupled with large elastic anisotropy [17,20−22].

CuAlNi alloy can exhibit shape memory properties only if the martensitic transformation took place. In order to ensure the undercooling necessary to enforce the martensitic transformation, in general, a heat treatment cannot be avoided [23]. The most common heat treatment of CuAlNi alloy is annealing in β-phase region, followed by subsequent water quenching [16,23]. Some works deal with the influence of heat treatment of CuAlNi alloy and similar alloys on the microstructure [23−25], and surface fracture morphology [26] but investigations about influence of heat treatment on corrosion behaviour of CuAlNi alloy are scarce. This work deals with the investigations of corrosion behaviour changes of the CuAlNi alloy as a result of heat treatment.

2 Experimental

CuAlNi alloy with composition of 83.1% Cu, 12.8% Al and 4.1% Ni (mass fraction) was produced by vertical continuous casting method in the shape of cylindrical rod with 8 mm in diameter. After casting, the alloy was subjected to heat treatment procedure containing solution annealing and tempering. Solution annealing was performed at 850, 885 and 920 °C for 60 min (sample K1, K2, and K3) and water quenching in room temperature water. Afterwards, the alloy was tempered at 300 °C for 60 min and then rapidly cooled in room temperature water. The working electrodes were prepared by machining the CuAlNi samples (in an as-cast state without and after heat treatment) into cylinders and soldered with insulated copper wire to ensure good electrical contact. After that, cylindrical samples were embedded in Polirepar S acrylate leaving only a circular disk exposed to the electrolyte (area of 0.5 cm^2). The electrolyte was 0.9% NaCl solution prepared by dissolving analytical grade NaCl salt in deionised water. The pH of the solution was adjusted to value of 7.4 with NaOH solution. Argon was bubbled through the NaCl solution 20 min prior to electrode immersion in the electrolyte as well as during the immersion period.

Experiments were performed in a double walled three-electrode glass cell thermostated at 37 °C, with Pt-plate auxiliary electrode and saturated calomel electrode (SCE) as a reference electrode, which was located in the Luggin capillary.

Before each experiment, the electrode surface was mechanically treated with different grit emery papers (from 400 to 1500), polished with Al_2O_3 polishing paste (particle size of 0.05 μm), ultrasonically degreased in ethanol, rinsed with deionised water, and immersed in electrolyte solution.

All electrochemical measurements were performed with a PAR 273A potentiostat/galvanostat and a PAR M5210 lock-in amplifier for electrochemical impedance spectroscopy (EIS) measurements.

The evaluation of corrosion behaviour of CuAlNi alloy in 0.9% NaCl solution was performed by open circuit potential measurements (φ_{OC}) in 60 min time period, linear polarisation method in the potential region of ±20 mV around corrosion potential, with the scanning rate of 0.2 mV/s and potentiodynamic polarisation method in the potential region of −0.250 V from open circuit potential to 1.100 V with the scanning rate of 0.5 mV/s.

The electrochemical impedance spectroscopy measurements were carried out at φ_{OC} using the signal amplitude of 10 mV and a frequency interval from 0.01 Hz to 50 kHz.

After corrosion testing, the surface of investigated samples was photographed by a Canon Ixus 1000 HS digital camera. The surface morphology of the samples before and after the potentiodynamic measurements was examined in detail by scanning electron microscope (SEM) JEOL JSM−5610. The quantitative analysis of the elements on the electrode surface was determined by energy dispersive spectroscopy (EDS). Identification of the chemical composition of surface corrosion products was carried out using a Shimadzu XRD−6000 diffractometer fitted with a Cu K_α X-ray source.

3 Results and discussion

The open circuit potential changes for all the studied CuAlNi electrodes in 0.9% NaCl solution are shown in Fig. 1. The steady state is reached within 60 min of electrode immersion in the electrolyte. It can be seen that there is no significant difference in values of open circuit potential for CuAlNi alloy in as-cast state compared with heat treated samples so heat treatment doesn't have influence on open circuit potential.

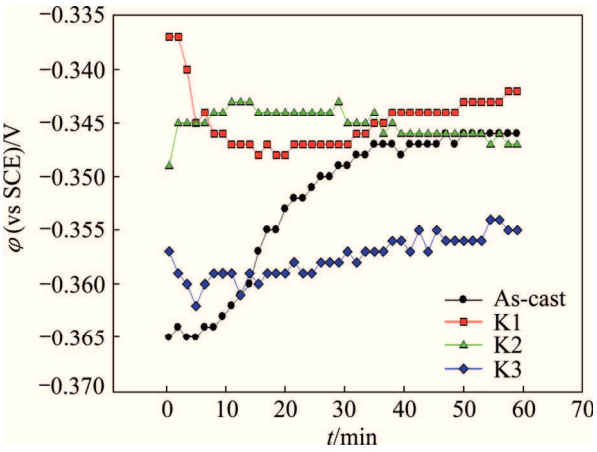

Fig. 1 Open circuit potential changes for CuAlNi alloy in 0.9% NaCl solution

Electrochemical impedance spectra were taken after the attainment of a stable open-circuit potential and the results are shown at Fig. 2 in Nyquist and Bode complex plane. Analysis of the results was performed using the algorithm developed by BOUKAMP [27]. Two slightly separate capacitive loops are observed in Nyquist complex plane, one in high frequency region and the other in low frequency region. These loops describe anodic partial reaction of dissolving Cu and mass transfer through the surface layer of corrosion products. The time constant at high frequencies is a result of modulation CuCl adsorbed layer on the surface of the electrode, while the low-frequency part of the diagram describes the diffusion processes at the electrode, or transfer of $CuCl_2$ ions through the layer on the electrode surface. Observed time constants are partially overlapping and in such graphic representation it is difficult to gain a clear insight into the results.

Bode plots (Fig. 2(b)) are recommended as standard impedance plots, since all experimental impedance data are equally represented and the phase angle as a sensitive parameter to interfacial phenomena appears explicitly [28]. This diagram shows the dependence of the absolute value of impedance and phase shift on the frequency. In the high frequency region (f>1 kHz), the influence of the electrolyte resistance R_{el} is dominant on the total impedance, and a phase shift between current and voltage is 0°. In the medium frequency region (f<1 kHz), the capacitive behaviour of electrodes is determined by dielectric properties of the phase layer on the electrode surface (phase shift is around 70°). In this area, linear lg $|Z|$ vs lg f relationship is observed with slope close to −1. In low frequency region, a linear dependence of the impedance on the frequency is observed, with a slope close to −0.5.

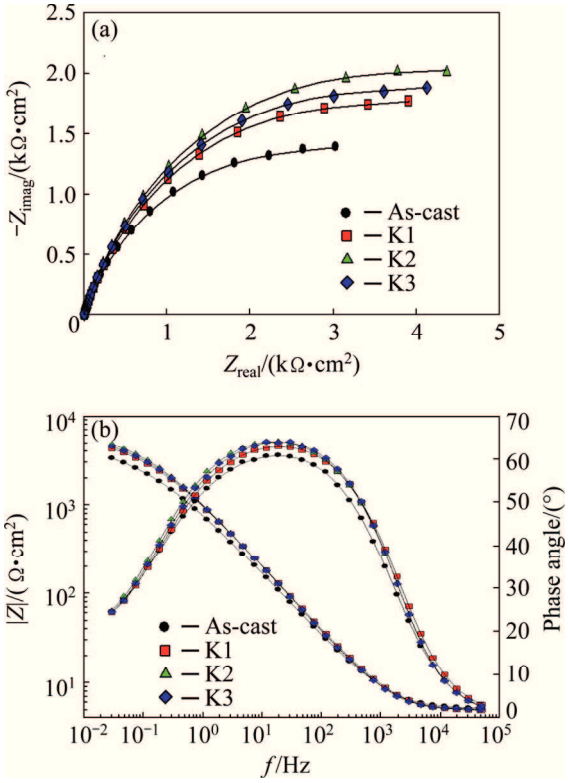

Fig. 2 Nyquist (a) and Bode (b) plots for CuAlNi alloy in 0.9% NaCl solution

The equivalent circuit used to fit the experimental results was shown elsewhere [15]. It consists of electrolyte resistance (R_{el}) which is connected with two time constants. The first time constant is determined by the parallel connection of a constant phase element and resistance, i.e., (Q_1R_1), while the second time constant represents a serial-parallel circuit of constant phase element (CPE), the resistance and the diffusion coefficient ($Q_2(R_2W)$). Time constant, Q_1R_1, observed in the high frequency region, is the result of the rapid process of charge transfer reaction in the dissolving of alloy in NaCl solution. In this case, R_1 represents a charge transfer resistance, and Q_1 is replaced by the capacity of the electrochemical double layer. The time constant in the low frequency area is a result of mass transfer (mainly Cu ions) through the surface film of corrosion products: Q_2 represents the capacitance of the film surface, R_2 is the resistance of the surface of the

film, and W is the diffusion element.

The constant phase element is related to the impedance (Z) according to the equation:

$$Z_{CPE}=[Q(j\omega)^n]^{-1} \quad (1)$$

where j is the imaginary root, ω is the applied frequency, and n is an exponential term.

CPEs are used in the analysis of impedance data to account deviations produced by surface roughness [29].

The calculated equivalent circuit parameters for CuAlNi alloy samples (in as-cast state and after quenching) are presented in Table 1.

Table 1 EIS data of CuAlNi alloy in as-cast and quenched state in 0.9% NaCl solution

Sample	R_{el}/ ($\Omega\cdot cm^2$)	Q_1/($10^6\ \Omega^{-1}\cdot S^n\cdot cm^{-2}$)	n_1	R_1/ ($\Omega\cdot cm^2$)
As-cast	5.07	85.73	0.85	17.03
K1	4.77	69.99	0.86	21.54
K2	4.96	63.83	0.88	24.28
K3	4.89	65.04	0.88	23.16

Sample	Q_2/($10^6\ \Omega^{-1}\cdot S^n\cdot cm^{-2}$)	n_2	R_2/ ($k\Omega\cdot cm^2$)	W/($10^3\ \Omega^{-1}\cdot S^n\cdot cm^{-2}$)
As-cast	259.73	0.61	3.93	2.64
K1	190.42	0.63	4.87	2.03
K2	182.59	0.65	5.48	1.87
K3	187.07	0.64	5.11	1.92

The results obtained indicate that heat treatment of CuAlNi alloy leads to a corresponding increase of charge transfer resistance (R_1) and surface layer resistance (R_2), while the capacitance of the double layer (Q_1), capacitance of the surface layer (Q_2) and the diffusion element (W) decrease, indicating higher corrosion resistance compared with CuAlNi alloy in the cast state (before heat treatment).

After impedance measurements, the linear polarisation measurements were performed, in the potential region of ±20 mV around φ_{OC} and the results are shown on Fig. 3. Polarisation resistance (R_p) represents the resistance of metal to corrosion, and is defined by the slope of the polarisation curve near the corrosion potential:

$$R_p=\Delta\varphi/\Delta J \quad (2)$$

The values of corrosion resistance for the CuAlNi samples are given in Table 2.

From Fig. 3, it can be seen that heat treatment leads to increase the slopes of the polarisation curves, resulting in higher values of R_p, which means higher resistance of CuAlNi alloy to corrosion. The increase in polarisation resistance values of heat treated CuAlNi alloy (K1, K2, and K3) suggests beneficial influence of heat treatment on corrosion resistance of CuAlNi alloy.

Potentiodynamic polarisation behaviour of the CuAlNi alloys without and with heat treatment in 0.9% NaCl solution is presented in Fig. 4.

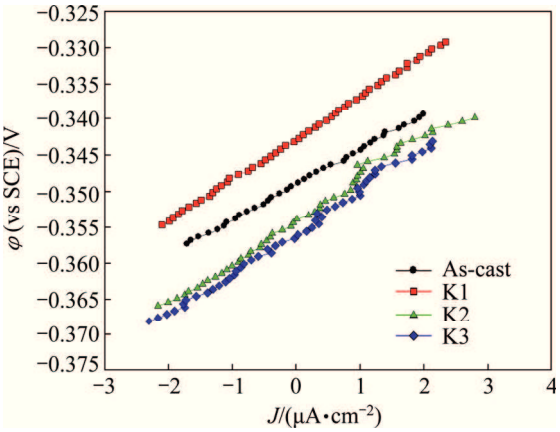

Fig. 3 Linear polarization curves for CuAlNi alloy in 0.9% NaCl solution

Table 2 Corrosion parameters for CuAlNi alloy in as-cast and quenched state in 0.9% NaCl solution

Sample	J_{corr}/ ($\mu A\cdot cm^{-2}$)	φ_{corr} (vs SCE)/V	R_p/ ($k\Omega\cdot cm^{-2}$)	v_{corr}/ ($mm\cdot a^{-1}$)
As-cast	2.84	−0.372	4.805	0.0313
K1	2.32	−0.377	5.934	0.0256
K2	2.18	−0.375	5.985	0.0242
K3	1.75	−0.378	5.850	0.0193

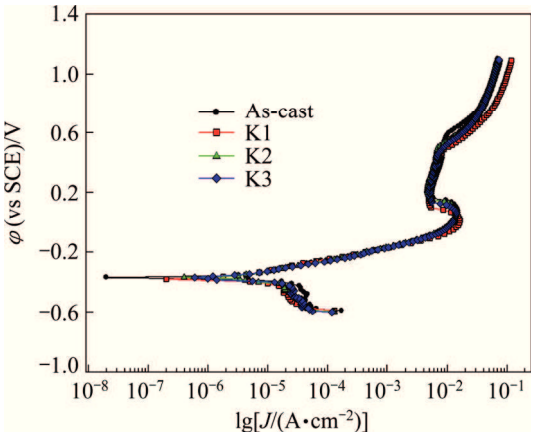

Fig. 4 Potentiodynamic polarization curves for CuAlNi alloy in 0.9% NaCl solution

Potentiodynamic polarisation curve is composed of two branches: cathodic branch, which is the result of occurring cathodic reaction and the anode part which is the result of occurring the anodic reaction, and in this case, alloy dissolution. Cathodic parts of polarisation curves should reflect hydrogen evolution reaction due to deaeration of the solution with Ar, 20 min before

immersion of electrode in electrolyte, as well as slow deaeration during investigation. Anodic parts of the curve describe corrosion of CuAlNi alloy can be divided into three regions: the apparent Tafel region, a region where there is a tendency of the electrode to passivate, and the third region in which the current density rises again with positive potential changes [15,30]. Tafel region is characterised by dissolution of Cu and Al from the alloy surface and the formation of complexes ($CuCl^{2-}$) that diffuse from the surface of the electrode in a solution, which is confirmed in the literatures [5,30]. Anodic current density reduction in active−passive region, can be explained by the formation of the surface corrosion products, probably cuprous chloride (CuCl) and cuprous oxide (Cu_2O), which have some protective effect and reduce the active dissolution of metals from the surface [15,30,31], or the formation of aluminium oxide/hydroxide layer, which has been found in the similar corrosion investigation on the surface of Cu−Al and Cu−Al−Ag alloys in 0.5 mol/L NaCl solution [29]. Further potential increase leads to destruction of corrosion products surface layer and the current density begins to rise again and the copper dissolution continues due to the formation of Cu(II) species [32]. By comparing the potentiodynamic polarisation curves for CuAlNi alloys (before and after heat treatment), very similar corrosion behaviour in NaCl solution can be seen for all investigated samples. The anodic parts of the curves in Tafel area almost complete overlap for all samples. In the active−passive area, anodic current density has slightly lower values for heat-treated CuAlNi alloys. However, because of dissolution of corrosion products from the electrode surfaces in third area, the opposite effect was visible, wherein the anodic current densities are somewhat greater for the heat treated samples compared with the as-cast CuAlNi sample. The maximum values of anodic current density in this area were observed for CuAlNi alloy tempered at 850 °C. The values of corrosion potential (φ_{corr}) are almost the same for all investigated CuAlNi samples. Corrosion rate is calculated according to [33]

$$v_{corr} = \frac{J_{corr} \cdot m_e}{\rho \cdot F} \quad (3)$$

where v_{corr} is the corrosion rate, cm/s; J_{corr} is the corrosion current density, A/cm^2; m_e is the equivalent mass of corroded alloy, g/mol; ρ is the density of CuAlNi alloy (7.1 g/cm^3); F is the Faraday constant (96485 J).

The beneficial effect of heat treatment is clearly visible from the lower values of corrosion current density of heat-treated samples and consequently the lower values of corrosion rate.

After the potentiodynamic measurement, the electrodes were taken from the cell and left dry in desiccator. Afterwards, the surface of the alloys was photographed in macro mode with digital camera Canon Ixus 1000 HS (Fig. 5). On all samples of CuAlNi alloy,

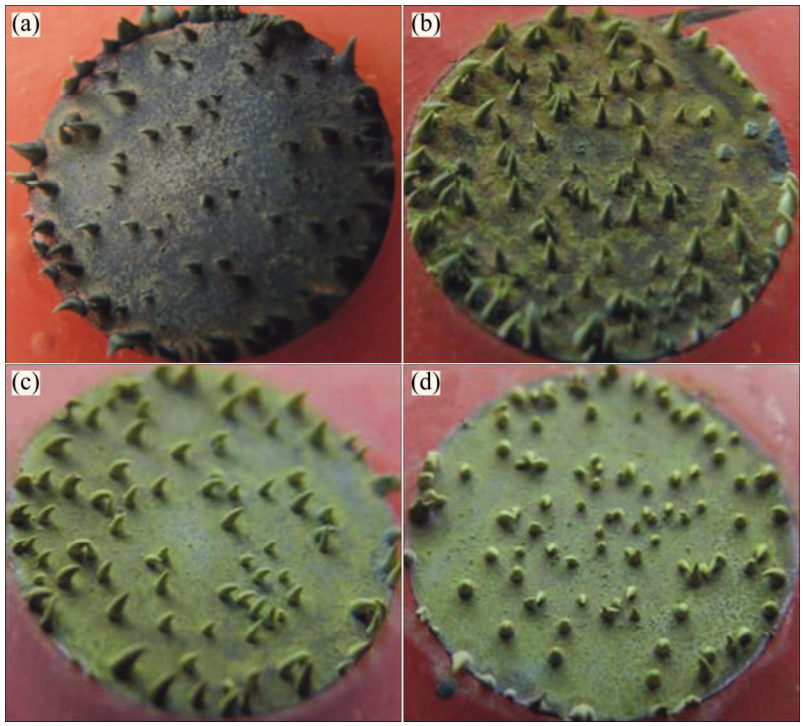

Fig. 5 Photographs of corrosion products in form of spikes on surface of CuAlNi samples after potentiodynamic polarization measurements: (a) As-cast; (b) K1; (c) K2; (d) K3

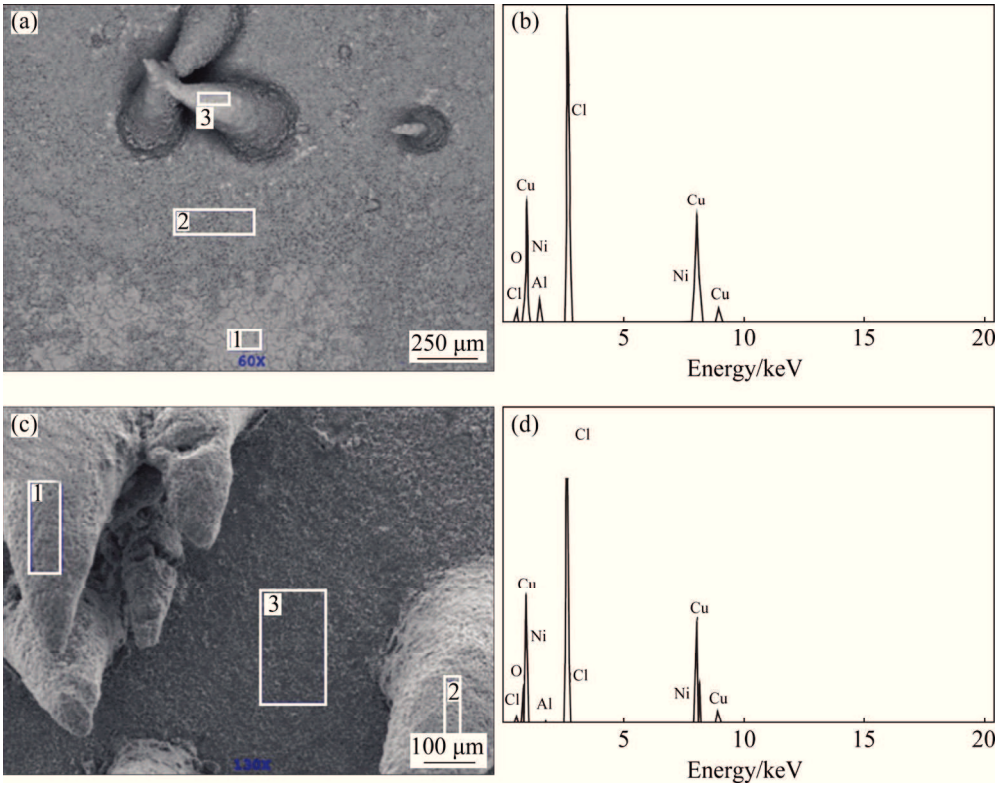

Fig. 6 SEM micrographs of CuAlNi alloy after potentiodynamic polarization measurements: (a) Surface morphology of sample K1 with marked positions for EDS analysis; (b) EDS spectrum for Position 1 in (a); (c) Surface morphology of sample K3 with marked positions for EDS analysis; (d) EDS spectrum for Position 1 in (c)

Table 3 EDS analysis results of chemical composition of corrosion surface layers on CuAlNi alloy after quenching

Sample	Position	*w*(Cu)/%	*w*(Al)/%	*w*(Ni)/%	*w*(Cl)/%	*w*(O)/%
K1	1	58.31	3.20	0.92	32.08	5.48
	2	68.48	1.04	0.63	24.90	4.96
	3	61.88	0.04	0.11	34.52	3.44
K3	1	64.43	0.01	0.10	33.98	1.49
	2	59.82	0.02	0.06	37.88	2.22
	3	64.05	0.65	0.45	30.93	3.92

deposits of corrosion products in the form of spikes can be observed mostly at the edge of the electrode surface and sporadically on the inner surface of the electrode. Detail surface morphology was examined by scanning electron microscope equipped with energy dispersive spectroscope (EDS), and the results are shown in Fig. 6.

In SEM micrographs, the surface morphology of the corrosion product can be observed (Figs. 6(a) and (c)). EDS analysis reveals elementary composition of the corrosion products on the surface of CuAlNi electrodes, which is given in Table 3. In the corrosion surface layer, dominant elements are Cu and Cl, with small amounts of O, Al, and Ni.

The X-ray diffraction patterns of CuAlNi alloy after the polarisation measurements are shown in Fig. 7. The existence of $CuCl_2$, $AlCl_3$ and $Cu_2Cl(OH)_3$ compounds in

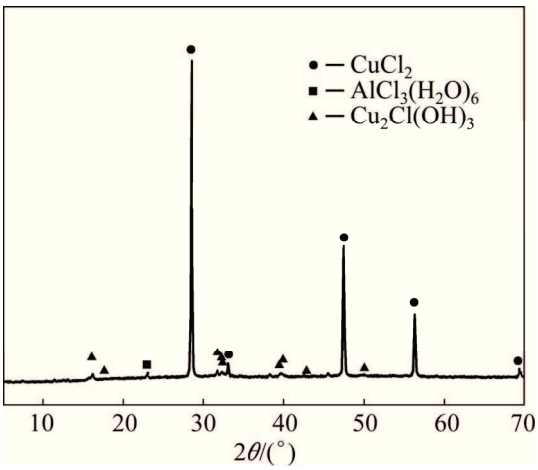

Fig. 7 XRD spectrum of CuAlNi alloy covered with corrosion surface layer

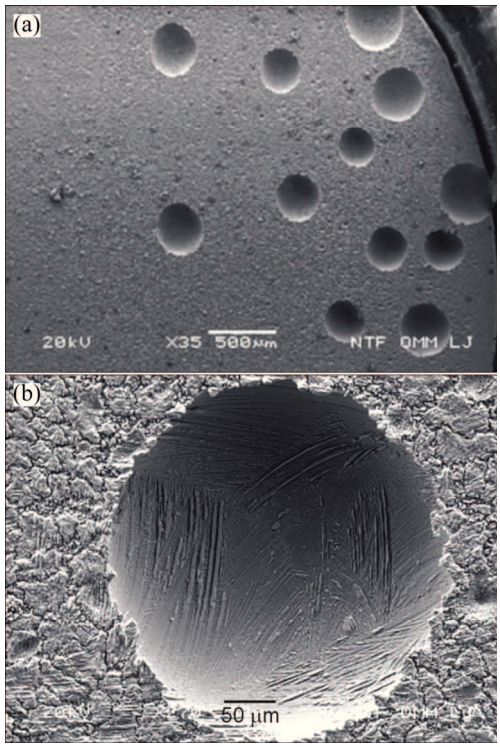

Fig. 8 SEM micrographs of CuAlNi alloy after removal corrosion product from electrode surface

the surface corrosion product further confirms the results of EDS analysis.

After removal of the corrosion products from the surface by ultrasonic treatment in deionized water, clearly visible pits that are formed by pitting corrosion appear on the electrode surface (Fig. 8).

4 Conclusions

1) Increase in polarisation resistance values of heat-treated CuAlNi alloy suggests beneficial influence of heat treatment (850−920 °C, 60 min and water quenching) on corrosion resistance of CuAlNi alloy in NaCl solution.

2) The results of potentiodynamic polarisation measurements have shown the almost identical values of corrosion potentials and slightly lower value of corrosion current for heat-treated CuAlNi alloy.

3) Results of electrochemical impedance spectroscopy measurements have shown that heat treatment of CuAlNi alloy leads to increase in values of charge transfer resistance and resistance of surface layers and decrease in values of constant phase element of the surface layer, which indicates better corrosion resistance.

4) Scanning electron microscopy analysis has shown the occurrence of pitting corrosion on the electrode surfaces. The spikes of corrosion product, and pits underneath the spikes, are concentrated on the edges of electrode. EDS analysis revealed elementary composition of the corrosion products on the surface of CuAlNi electrodes, which consist of Cu and Cl as dominant elements along with small amounts of O, Al and Ni.

5) The X-ray diffraction patterns of CuAlNi alloy show the existence of $CuCl_2$, $AlCl_3$ and $Cu_2Cl(OH)_3$ in the surface corrosion product.

6) After removal of the corrosion products from the alloy surface, clearly visible pits appear on the electrode surface.

Acknowledgements

This work has been fully supported by the Croatian Science Foundation under the project IP-2014-09-3405.

References

[1] ABOUSWA K, ELSHAWESH F, ELRAGEI O, ELHOOD A. Corrosion investigation of Cu−Ni tube desalination plant [J]. Desalination, 2007, 205: 140−146.

[2] MAO Xiang-yang, FANG Feng, JIANG Jian-qing, TAN Rong-sheng. Effect of rare earths on corrosion resistance of Cu−30Ni alloys in simulated seawater [J]. Journal of Rare Earths, 2009, 27: 1037−1041.

[3] VRSALOVIĆ L, OGUZIE E E, KLIŠKIĆ M, GUDIĆ S. Corrosion inhibition of CuNi10Fe alloy with phenolic acids [J]. Chemical Engineering Communication, 2011, 198: 1380−1393.

[4] BADAWY W E, EL-SHERIF R M, SHEHATA H. Electrochemical stability of Cu−10Al−5Ni alloy in chloride-sulfate electrolytes [J]. Electrochimica Acta, 2009, 54: 4501−4505.

[5] SAUD S N, ABUBAKAR H T, BAKHSHESHI-RAD H R. Microstructure and corrosion behavior of Cu−Al−Ni shape memory alloys with Ag nanoparticles [J]. Materials and Corrosion, 2015, 66: 527−534.

[6] SAUD S N, HAMZAH E, ABUBAKAR T, BAKHSHESHI-RAD H R. Correlation of microstructural and corrosion characteristics of quaternary shape memory alloys Cu−Al−Ni−X (X=Mn or Ti) [J]. Transactions of Nonferrous Metals Society of China, 2015, 25: 1158−1170.

[7] KUO H H, WANG W H, HSU Y F, HUANG C A. The corrosion behavior of Cu−Al and Cu−Al−Be shape memory alloys in 0.5 M H_2SO_4 solution [J]. Corrosion Science, 2006, 48: 4352−4364.

[8] HUSAIN S W, CLAPP P C. The effect of aging on the fracture behavior of Cu−Al−Ni β phase alloys [J]. Metallurgical and Materials Transactions A, 1988, 19: 1761−1766.

[9] SATHISH S, MALLIK U S, RAJU T N. Microstructure and shape memory effect of Cu−Zn−Ni shape memory alloys [J]. Journal of Minerals and Materials Characterization and Engineering, 2014, 2: 71−77.

[10] DASGUPTA R. A look into Cu-based shape memory alloys: Present scenario and future prospects [J]. Journal of Materials Research, 2014, 29: 1681−1698.

[11] GUSTMANN T, DOS SANTOS J M, GARGARELLA P, KÜHN U, VAN HUMBEECK J, PAULY S. Properties of Cu-based shape-memory alloys prepared by selective laser melting [J]. Shape Memory and Superelasticity, 2017, 3: 24−36.

[12] MANJAIAH M, NARENDRANATH S, BASAVARAJAPPA S. Review on non-conventional machining of shape memory alloys [J]. Transactions of Nonferrous Metals Society of China, 2014, 24: 12−21.

[13] LAGOUDAS D C. Shape memory alloys modeling and engineering

applications [EB/OL]. New York: Springer, 2008. DOI: 10.1007/978-0- 387-47685-8

[14] KNEISSL A C, UNTERWEGER E, BRUNCKO M, LOJEN G, MEHRABI K, SCHERNGELL H. Microstructure and properties of NiTi and CuAlNi shape memory alloys [J]. Metallurgical & Materials Engineering, 2008, 14: 89−100.

[15] GOJIĆ M, VRSALOVIĆ L, KOŽUH S, KNEISSL A, ANŽEL I, GUDIĆ S, KOSEC B, KLIŠKIĆ M. Electrochemical and microstructural study of the Cu−Al−Ni shape memory alloy [J]. Journal of Alloys and Compounds, 2011, 509: 9782−9790.

[16] IVANIĆ I, GOJIĆ M, KOŽUH S. Shape memory alloys (Part II): Classification, production and application [J]. Chemistry in Industry, 2014, 63: 331−344. (in Croatian)

[17] SARI U. Influences of 2.5wt% Mn addition on the microstructure and mechanical properties of Cu−Al−Ni shape memory alloys [J]. International Journal of Minerals, Metallurgy and Materials, 2010, 17: 192−198.

[18] ČOLIĆ M, RUDOLF R, STAMENKOVIĆ D, ANŽEL I, VUČEVIĆ D, JENKO M, LAZIĆ V, LOJEN G. Relationship between microstructure, cytotoxicity and corrosion properties of Cu−Al−Ni shape memory alloy [J]. Acta Biomaterialia, 2010, 6: 308−317.

[19] ZARE M, KETABCHI M. Effect of chromium element on transformation, mechanical and corrosion behavior of thermomechanically induced Cu−Al−Ni shape-memory alloys [J]. Journal of Thermal Analysis and Calorimetry, 2017, 127: 2113−2123.

[20] MOGHADDAM A O, KETABCHI M, BAHRAMI R. Kinetic grain growth, shape memory and corrosion behavior of two Cu-based shape memory alloys after thermomechanical treatment [J]. Transactions of Nonferrous Metals Society of China, 2013, 23: 2896−2904.

[21] SHARMA M, VAJPAI S K, DUBE R K. Synthesis and properties of Cu−Al−Ni shape memory alloy strips prepared via hot densification rolling of powder preforms [J]. Powder Metallurgy, 2011, 54: 620−627.

[22] IZADINIA M, DEHGHANI K. Structure and properties of nanostructured Cu−13.2Al−5.1Ni shape memory alloy produced by melt spinning [J]. Transactions of Nonferrous Metals Society of China, 2011, 21: 2037−2044.

[23] LOJEN G, ANŽEL I, KNESSL A, KRIŽMAN A, UNTERWEGER E, KOSEC B, BIZJAK M. Microstructure of rapidly solidified Cu−Al−Ni shape memory alloy ribbons [J]. Journal of Materials Processing Technology, 2005, 162−163: 220−229.

[24] SAKAMOTO H, SHIMIZU K. Effect of heat treatments on thermally formed martensite phases in monocrystalline Cu−Al−Ni shape memory alloy [J]. ISIJ International, 1989, 29: 395−403.

[25] SLAMA P, DLOUHY J, KOVER M. Influence of heat treatment on the microstructure and mechanical properties of aluminium bronze [J]. Materials and Technology, 2014, 48: 599−604.

[26] IVANIĆ I, KOŽUH S, KOSEL F, KOSEC B, ANŽEL I, BIZJAK M, GOJIĆ M. The influence of heat treatment on fracture surface morphology of the CuAlNi shape memory alloy [J]. Engineering Failure Analysis, 2017, 77: 85−92.

[27] BOUKAMP B A. Equivalent circuit – User's manual [M]. Ver. 4.55. University of Twente, 1997: 1−53.

[28] BADAWY W A, ISMAIL K M, FATHI A M. Corrosion control of Cu−Ni alloys in neutral chloride solutions by amino acids [J]. Electrochimica Acta, 2006, 51: 4182−4189.

[29] BENEDETTI A V, SUMODJO P T A, NOBE K, CABOT P L, PROUD W G. Electrochemical studies of copper, copper-aluminium and copper-aluminium-silver alloys: impedance results in 0.5 M NaCl [J]. Electrochimica Acta, 1995, 40: 2657−2668.

[30] de SALAZAR J M G, SORIA A, BARRENA M I. Corrosion behaviour of Cu-based shape memory alloys, diffusion bonded [J]. Journal of Alloys and Compounds, 2005, 387: 109−114.

[31] ALFANTAZI A M, AHMED T M, TROMANS D. Corrosion behavior of copper alloys in chloride media [J]. Materials and Design, 2009, 30: 2425−2430.

[32] KEAR G, BARKER B D, WALSH F C. Electrochemical corrosion of unalloyed copper in chloride media—A critical review [J]. Corrosion Science, 2004, 46: 109−135.

[33] BABOLAN R. Corrosion tests and standards, applications and interpretations [M]. 2 nd ed. USA: ASTM International, 2005.

热处理对 CuAlNi 形状记忆合金腐蚀性能的影响

L. VRSALOVIĆ[1], I. IVANIĆ[2], S. KOŽUH[2], S. GUDIĆ[1], B. KOSEC[3], M. GOJIĆ[2]

1. Department of Electrochemistry and Materials Protection, Faculty of Chemistry and Technology, University of Split, Ruđera Boškovića 35, 21000 Split, Croatia;
2. Faculty of Metallurgy, University of Zagreb, Aleja narodnih heroja 3, 44103 Sisak, Croatia;
3. Faculty of Natural Sciences and Engineering, University of Ljubljana, Aškerčeva cesta 12, 1000 Ljubljana, Slovenia

摘　要：通过开路电位测试、 极化技术和电化学阻抗谱法研究热处理对 CuAlNi 形状记忆合金腐蚀性能的影响，测试条件为：0.9% NaCl 溶液，pH=7.4 和 *T*=37 °C。对比研究铸态和分别在 850、885 和 920 °C 退火+水冷淬火后的 CuAlNi 合金样品。电化学阻抗谱法的结果显示，热处理后的 CuAlNi 合金其电荷转移电阻和表层电阻增加、双层表面和表层电容值降低，说明与铸态合金相比，热处理提高了合金的耐腐性。极化电阻的增加和腐蚀电流密度的降低也表明热处理对 CuAlNi 合金的耐腐蚀性能有利。对极化曲线测试后的样品表面进行光学显微镜、SEM/EDX 和 XRD 分析。结果表明，电极表面发生点蚀，腐蚀产物为 $CuCl_2$、$AlCl_3$ 和 $Cu_2Cl(OH)_3$。

关键词：CuAlNi 合金；腐蚀；极化；电化学方法；SEM

(Edited by Bing YANG)